Acta Crystallographica Section D
Biological Crystallography
ISSN 0907-4449

Structural insights into a zinc-dependent pathway leading to Leu55Pro transthyretin amyloid fibrils

Artur F. Castro-Rodrigues,[a] Luís Gales,[a,b] Maria J. Saraiva[a,b] and Ana M. Damas[a,b]*

[a]IBMC – Instituto de Biologia Molecular e Celular, Universidade do Porto, Porto, Portugal, and [b]ICBAS – Instituto de Ciências Biomédicas de Abel Salazar, Universidade do Porto, Porto, Portugal

Correspondence e-mail: amdamas@ibmc.up.pt

Received 13 September 2011
Accepted 26 October 2011

PDB Reference: TTR L55P–Zn^{2+} complex, 3ssg.

Human transthyretin (TTR) is a homotetrameric protein that is responsible for the formation of amyloid in patients with familiar amyloidotic polyneuropathy (FAP), familiar amyloidotic cardiomyopathy (FAC) and senile systemic amyloidosis (SSA). Amyloid fibrils are characterized by a cross-β structure. However, details of how TTR monomers are organized to form such an assembly remain unknown. The effect of Zn^{2+} in increasing TTR L55P amyloidogenecity has been reported. Crystals of the TTR L55P–Zn^{2+} complex were grown under conditions similar to those leading to higher amyloidogenic potential of the variant protein and the three-dimensional structure of the complex was determined by X-ray crystallography. Two different tetrahedral Zn^{2+}-binding sites were identified: one cross-links two tetramers, while the other lies at the interface between two monomers in a dimer. The association of monomers involving the two Zn^{2+}-binding sites leads to a bidimensional array with a cross-β structure. The formation of this structure and subsequent organization into amyloid fibrils was monitored by fluorescence spectroscopy and electron microscopy. The TTR L55P–Zn^{2+} structure offers the first molecular insights into the role of Zn^{2+} as a mediator of cross-β-type structure in TTR amyloidosis and the relevance of a Zn^{2+}-dependent pathway leading to the production of early amyloidogenic intermediates is discussed.

1. Introduction

Human plasma transthyretin (TTR) is a transport protein of thyroxin (T_4), by direct binding, and of retinol (vitamin A) when in complex with the retinol-binding protein (RBP) (Raz & Goodman, 1969). While wild-type TTR (wt TTR) is present in extracellular amyloid deposits occurring mainly in the heart of elderly people suffering from systemic senile amyloidosis (SSA; Westermark *et al.*, 1990), patients carrying amyloidogenic single-residue TTR variants show disease symptoms that are associated with familial amyloidotic cardiomyopathy (FAC) and with familial amyloidotic polyneuropathy (FAP) (Andrade, 1952). Nearly 100 different TTR mutations have been described, with the majority being associated with amyloidosis (Saraiva, 2001). Among the reported mutations, the TTR L55P variant has been described as the most aggressive, since it is associated with early onset of the disease and involves cardiac and neurologic pathologies (Jacobson *et al.*, 1992).

TTR is a homotetramer with 222 molecular symmetry. Each monomer consists of a β-sandwich with two four-stranded β-pleated sheets, referred to as *DAGH* and *CBEF*, and a

short α-helix between strands *E* and *F* (Blake *et al.*, 1978). The association of two TTR monomers leads to a dimer with an extended β-sandwich composed of two eight-stranded β-sheets (*DAGHH′G′A′D′* and *CBEFF′E′B′C′*), which are established through contacts between the *F* and *H* strands of different monomers. The interactions between the two TTR dimers that form the tetramer consist of a reduced number of hydrogen bonds and hydrophobic contacts. The dimers define a central channel that runs through the molecule, in which two equivalent binding sites for T_4 are located (Wojtczak *et al.*, 1996). The crystal structures of TTR L55P determined to date, in the apo form and as a complex with 2,4-dinitrophenol (DNP), showed that the overall tetrameric TTR structure is maintained, while the secondary structure of each monomer is affected by the disruption of the short edge strand *D*, leading to the formation of an extended loop between strands *C* and *E* (Sebastião *et al.*, 1998; Morais-de-Sá *et al.*, 2006; Cendron *et al.*, 2009). Engineered variants with mutations and deletions in strand *D* have also been reported to be highly amyloidogenic (Goldsteins *et al.*, 1997).

The cross-β structure present in amyloid fibrils constitutes a unifying structural motif common to amyloid deposits formed by several proteins (Sunde *et al.*, 1997). It consists of a linear arrangement of β-pleated sheets with the β-strands oriented perpendicularly to the fibril axis and backbone hydrogen bonding running parallel to it (Eanes & Glenner, 1968). Although this structural feature has been identified in *ex vivo* TTR amyloid fibrils extracted from tissues of FAP patients (Blake & Serpell, 1996; Inouye *et al.*, 1998), experimental data have not been sufficient to reveal the structural and molecular details of the fibrillar arrangement.

TTR L55P fibrils can be produced *in vitro* under physiological-like conditions akin to the dissociation of the tetramer in human plasma, namely at neutral pH after incubation at 310 K for a few weeks (Cardoso *et al.*, 2002). Fibrils assembled under these conditions display the amyloid-characteristic cross-β pattern, as revealed by X-ray diffraction analysis (Gales *et al.*, 2003). It is generally accepted that they are a consequence of the dissociation of the tetramer into monomers that become structurally different and prone to aggregation, constituting an array of fibril intermediates in the amyloid cascade of events (Lashuel *et al.*, 1999; Quintas *et al.*, 2001). Even though the L55P mutation is located at the edge of the molecule, the TTR L55P tetramer is more prone to dissociation (Sebastião *et al.*, 2000; McCutchen *et al.*, 1993). Accordingly, the inhibition of wt TTR fibril formation mediated by sulfite was associated with new interactions stabilizing the strand *D* region (Gales *et al.*, 2007). Moreover, the low T_4-binding affinity observed for this variant is probably a consequence of a larger T_4-binding channel (Almeida & Saraiva, 1996; Sebastião *et al.*, 1998). Since TTR L55P fibrils can be obtained under physiological-like conditions and crystals for TTR L55P structure determination were obtained from a solution with amyloid-like properties, it was proposed that the obtained TTR L55P model corresponds to an initial species in the amyloidogenesis cascade (Sebastião *et al.*, 2000).

The preferential accumulation of zinc in TTR amyloid fibrils of FAP patients has been reported (Susuki *et al.*, 2008). Furthermore, the effect of Zn^{2+} in promoting TTR L55P amyloid formation has also been described (Wilkinson-White & Easterbrook-Smith, 2007). These authors showed that the dissociation constant of Zn^{2+} bound to both wt TTR and TTR L55P lies within the low micromolar range of plasma Zn^{2+} levels (Ghayour-Mobarhan *et al.*, 2005; Susuki *et al.*, 2008), correlating with the previous identification of TTR as a serum Zn^{2+}-binding protein (Scott & Bradwell, 1983). The structural role of Zn^{2+} in an engineered monomeric variant of wt TTR and its implications for amyloidogenesis and retinol transport have recently been addressed (Palmieri *et al.*, 2010). A perturbation of the loop *E*–α-helix–loop *F* region has been described, as previously found in crystal structures of wt TTR at low pH in the absence of Zn^{2+} (Palaninathan *et al.*, 2008), which also led to a decrease of affinity for RBP.

In this work, we determined the crystal structure of TTR L55P in complex with Zn^{2+} at physiological pH to identify the molecular mechanism underlying the reported effect of Zn^{2+} on the amyloidogenic potential of this TTR variant. Furthermore, in order to correlate the structure of this complex with amyloid fibril growth, the amyloidogenicity of TTR L55P in a solution similar to that used to grow the TTR L55P–Zn^{2+} crystals was tested using the amyloid-specific probe thioflavin T (ThT) and analysed by electron microscopy.

2. Materials and methods

2.1. Protein expression and purification

The recombinant TTR L55P was expressed in *Escherichia coli* and isolated as reported previously (Furuya *et al.*, 1991). Purified samples of TTR L55P were dialysed against 10 m*M* HEPES pH 7.5 and concentrated to 8.5 mg ml^{-1}. The protein concentration was determined from the absorbance at 280 nm using the previously determined molar extinction coefficient of TTR (Raz & Goodman, 1969).

2.2. Crystallization

TTR L55P was crystallized by the hanging-drop vapour-diffusion technique at 287 K. The reservoir solution consisted of 3%(*w*/*v*) PEG 8000, 0.1 *M* cacodylate pH 6.5, 5 m*M* zinc acetate. The crystallization drops were set up by mixing the protein and reservoir solutions in 1:1 proportions. The TTR L55P nucleated within 1 h and by that time very small crystals were already visible. After a few hours, small crystals with defined morphology could be observed and they grew to maximum size after 2 d. Previous trials under similar crystallization conditions, using the same precipitant solution components but without zinc acetate, led only to microcrystals. In further trials screening the crystallization buffer very small crystals could be obtained in about a week, but were still unsuitable for X-ray analysis. Therefore, the obtained crystals are Zn^{2+}-dependent. After reaching maximum size, the TTR L55P–Zn^{2+} crystals were harvested and incubated in a drop of stabilizing solution containing 20%(*w*/*v*) glycerol immediately

Table 1
Data-collection and refinement statistics.

Values in parentheses are for the last shell.

Data collection	
Space group	$P4_22_12$
Unit-cell parameters (Å)	$a = b = 54.6$, $c = 86.6$
Resolution range (Å)	46.18–2.00
No. of observations	124430 (9418)
Multiplicity	13.2 (13.7)
R_{merge} (%)	5.8 (42.3)
Completeness (%)	100.0 (100.0)
$\langle I/\sigma(I)\rangle$	38.8 (9.0)
Matthews coefficient (Å^3 Da^{-1})	2.31
Solvent content (%)	46.7
Structure refinement	
R factor/R_{free} (%)	20.5/24.7
No. of unique reflections (working/test set)	8933/449
Water molecules	98
Residues with alternate conformations	Ser23, Ser46, Lys80, Thr119
Total No. of atoms	1004
Average B factors (Å^2)	
Overall	31.7
Protein	30.2
Main chain	29.1
Side chain	31.5
Water	44.1
Cacodylate	60.4
Zn^{2+}	30.8
R.m.s. bonded B factors (Å^2)	1.9
R.m.s. deviations from ideal values	
Bonds (Å)	0.012
Angles (°)	1.3
Ramachandran plot statistics (%)	
Most favoured regions	91.0
Additional allowed regions	8.0
Generously allowed regions	1.0

before flash-cooling in liquid nitrogen for subsequent X-ray diffraction data collection.

2.3. Structure determination

X-ray diffraction data were collected at 100 K using synchrotron radiation on beamline ID14-2 (λ = 0.933 Å), equipped with an ADSC Q4 CCD detector, at the European Synchrotron Radiation Facility (ESRF, Grenoble, France). Diffraction images were collected to a resolution of 1.8 Å. Two data sets were collected, with a shorter exposure time for the second set to cover the low-resolution diffraction. After indexing and integration of reflections, the two data sets were merged into a single set using *SORTMTZ* from the *CCP*4 suite (Winn *et al.*, 2011). Determination of the crystal orientation and integration of the reflections were carried out with *MOSFLM* (Leslie, 1992), and *SCALA* (Winn *et al.*, 2011) was used for the scaling and merging of integrated reflections. The structure-factor amplitudes were calculated from the intensities with *TRUNCATE* (Winn *et al.*, 2011). The data were processed and only reflections up to 2.0 Å resolution were used, since scaling statistics were poor for reflections beyond 2.0 Å and no improvement was observed in the electron-density maps when all reflections were included. Details of the diffraction data collection are presented in Table 1.

The structure of the TTR L55P–Zn^{2+} complex was solved by molecular replacement with *Phaser* (McCoy *et al.*, 2007), using as a search model the coordinates corresponding to the crystal structure of TTR L55P (Morais-de-Sá *et al.*, 2006; PDB entry 2b14, chain *A*). The initial model was then submitted to initial rigid-body refinement with *CNS* (Brunger, 2007) and both $2F_o - F_c$ and $F_o - F_c$ electron-density maps were generated and analysed. Subsequently, automated refinement was carried out with *REFMAC* (Winn *et al.*, 2011) alternated with manual model fitting and building with *Coot* (Emsley & Cowtan, 2004). The solvent water molecules, cacodylate buffer ion and Zn^{2+} metal ions were added manually in positive peaks of the $F_o - F_c$ electron-density maps. The initial $F_o - F_c$ difference map revealed highly intense electron density at the Zn^{2+} sites, especially at BS1, which also had coupled to it a highly intense electron-density blob that was interpreted as a cacodylate molecule coordinated to Zn^{2+}. After adding the Zn^{2+} ions to the initial TTR L55P model and one cycle of refinement, the $F_o - F_c$ map indicated the need to adjust the Zn^{2+} occupancies. The interatomic distances between the inter-tetramer Zn^{2+} and the coordinating cacodylate O atom O2 and between the intra-dimer Zn^{2+} and the coordinating Glu92 carboxylic O atom O1 were slightly restrained upon refinement according to the corresponding consensus reliable values derived from organic and inorganic deposited structures (Harding, 2006). Similarly, the interatomic distance between the Glu92 carboxylic O atom O2 and the Zn^{2+}-coordinating O atom from water H_2O86 was restrained considering a hydrogen-bond cutoff value of $\geq$2.6 Å. The quality of the final model was assessed using *PROCHECK* (Winn *et al.*, 2011), which showed that more than 90% of the TTR L55P residues are in the most favoured regions of the Ramachandran plot and that there are no amino acids in the disallowed regions. A summary of the relevant refinement statistics is presented in Table 1.

2.4. Preparation of amyloid fibrils

TTR L55P fibrils were produced under solution conditions similar to those in which crystals were grown (keeping the same Zn^{2+}:protein molar ratio), except for the absence of the precipitating agent. Solutions of TTR L55P (1.0 mg ml^{-1}) in 0.1 *M* cacodylate pH 6.5 in the presence or absence of 500 µ*M* zinc acetate were incubated at 310 K.

2.5. Thioflavin T-binding assay

The effect of Zn^{2+} on TTR L55P amyloid fibril formation was tested using the amyloid-specific fluorescent probe thioflavin T (ThT; Fluka). At increasing incubation times, 15 µl samples were taken for ThT fluorescence monitoring after mixing with ThT buffer (50 µ*M* ThT in 50 m*M* glycine–NaOH pH 9.0) to give a final volume of 150 µl. ThT excitation spectra were recorded at 298 K between 400 and 500 nm (using 1 nm increments) in a FluoroMax-4 (HORIBA Jobin Yvon) spectrofluorimeter, monitoring emission at 482 nm. Both excitation and emission slits were set to 5 nm.

2.6. Transmission electron microscopy (TEM)

The effect of Zn^{2+} on the growth of TTR L55P amyloid fibrils was monitored by TEM. At different incubation times, 5 µl aliquots were placed on a glow-discharged carbon-coated collodion film supported on 300-mesh copper grids and left to stand for a few minutes. Excess solution was then removed and after staining with 1% uranyl acetate the grids were analysed using a Zeiss EM902A electron microscope operating at 50 kV and equipped with an Orius (Gatan) camera interface.

3. Results

3.1. TTR L55P–Zn^{2+} overall structure

The TTR L55P–Zn^{2+} complex crystallized in the tetragonal space group $P4_22_12$ with one TTR L55P monomer in the asymmetric unit. Therefore, the TTR L55P tetramer has four structurally identical monomers all interrelated by three orthogonal twofold-symmetry axes (Fig. 1).

The final molecular model (PDB entry 3ssg) included amino acids 10–125, two Zn^{2+} ions, 98 water molecules and one cacodylate molecule from the buffer present in the crystallization solution. The water molecules were fitted into peaks with high density (>3σ) and good hydrogen-bond geometry. As is generally observed for N- and C-terminal residues in TTR crystal structures, residues 1–9 and 126–127 were disordered and could not be fitted into the electron density. The side chains of residues Ser23, Ser46, Lys80 and Thr119 were modelled in two different conformations. The Ramachandran plot (Table 1) showed that Asp39 is in a generously allowed region. The electron density for this residue is clearly defined and its unexpected geometry is probably owing to the positional restraint imposed by a crystal contact.

As observed in other TTR L55P structures, the TTR L55P–Zn^{2+} monomer consists of a β-sandwich formed by a four-stranded β-sheet *CBEF* and a three-stranded β-sheet *AGH*. Quaternary interactions led to the formation of the tetrameric biological unit displayed in Fig. 1. Comparisons of the intra-dimer main-chain hydrogen bonds at the monomer–monomer interfaces in the crystal structures of TTR L55P–Zn^{2+}, monoclinic apo TTR L55P (Sebastião *et al.*, 1998; PDB entry 5ttr), orthorhombic apo TTR L55P at neutral pH (Cendron *et al.*, 2009; PDB entry 3djz) and orthorhombic TTR L55P–DNP (Morais-de-Sá *et al.*, 2006; PDB entry 2b14) show that the TTR L55P–Zn^{2+} dimer has the same interactions as those previously described in the various TTR L55P structures. The water-bridged hydrogen bonds between the monomers that form a TTR dimer are also maintained in TTR L55P–Zn^{2+}. Interesting, however, is the additional main-chain Glu92–H_2O–Glu92^{symm} interaction which occurs owing to the presence of a novel water molecule at the TTR *FF′* interface. Since Glu92 is involved in the coordination of Zn^{2+}, its electron density is well defined, showing this water-mediated interaction between the two Glu92 amino acids and suggesting that Zn^{2+} may play a positive role in the stabilization of the

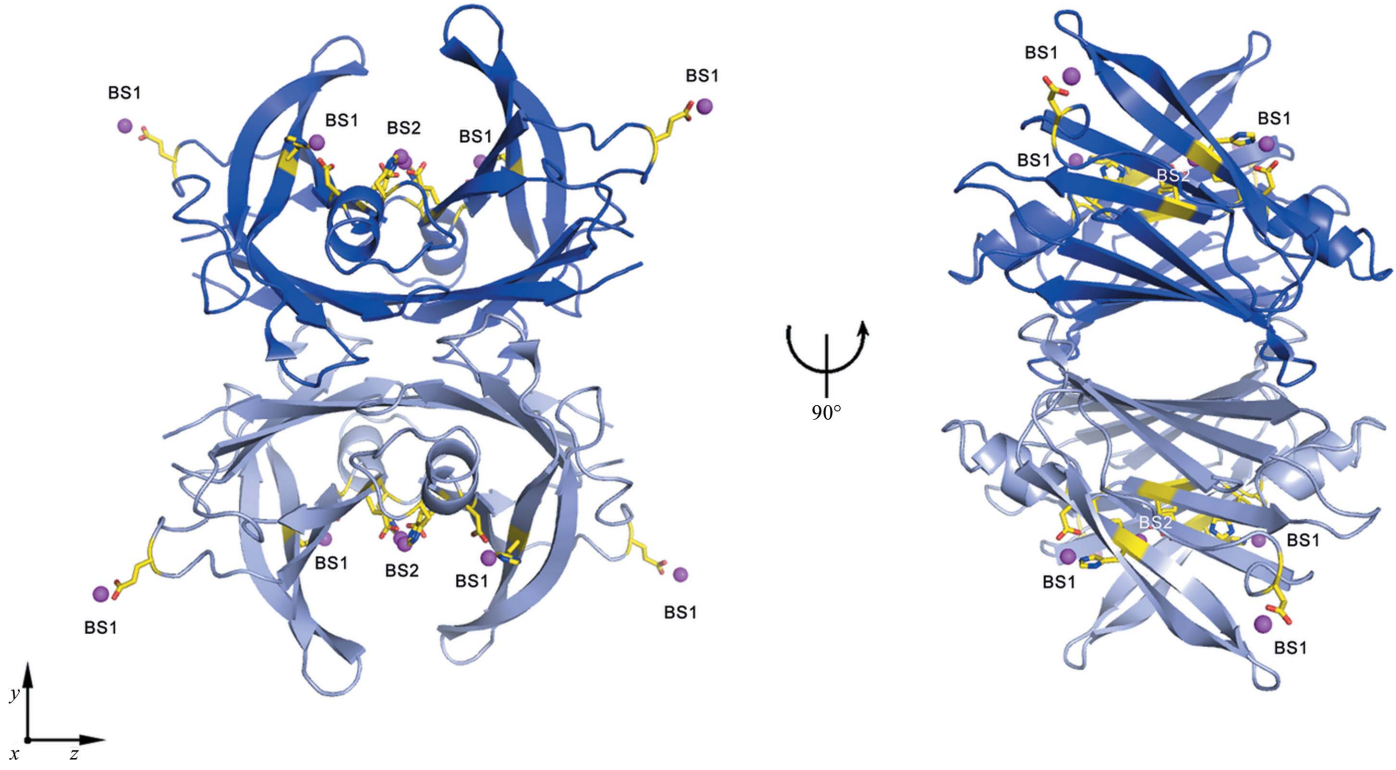

Figure 1
The crystallographic structure of the TTR L55P–Zn^{2+} complex. Two orthogonal orientations with a rotation along the molecular *y* axis are presented. The T_4-binding channel is clearly seen in the right panel (the *z* molecular axis runs along the channel). The Zn^{2+} ions are shown as magenta spheres and the side chains of the Zn^{2+}-coordinating residues are shown as sticks. The colour scheme matches that used in Fig. 2(*d*).

TTR L55P dimer by strengthening the interaction between monomers.

The overall structure of the TTR L55P–Zn^{2+} monomer is very similar to the previously determined structures for this variant (the maximum root-mean-square deviation for the main chain is 0.39 Å). It has been observed that loop *FG* (residues 98–103) has structural instability and its conformation is highly influenced by particular crystallographic contacts. In the TTR L55P–Zn^{2+} structure Gly101 makes van der Waals contacts with the same region of another tetramer, which contributes to the stabilization of the loop. Both loop *BC* (residues 36–41) and the C-terminal half of loop *CE* (residues 50–66) have amino acids involved in crystal contacts through hydrogen bonds and also, in the latter case, a Zn^{2+}-coordination bond. Moreover, Asp39 is conformationally restrained by the interaction with His56 of a neighbouring tetramer.

3.2. Zn^{2+}-binding sites

Two different Zn^{2+}-binding sites, both with tetrahedral geometry, were found in the crystal structure of TTR L55P–Zn^{2+}. One site is located at the interface of two monomers belonging to different tetramers (BS1), while the other site

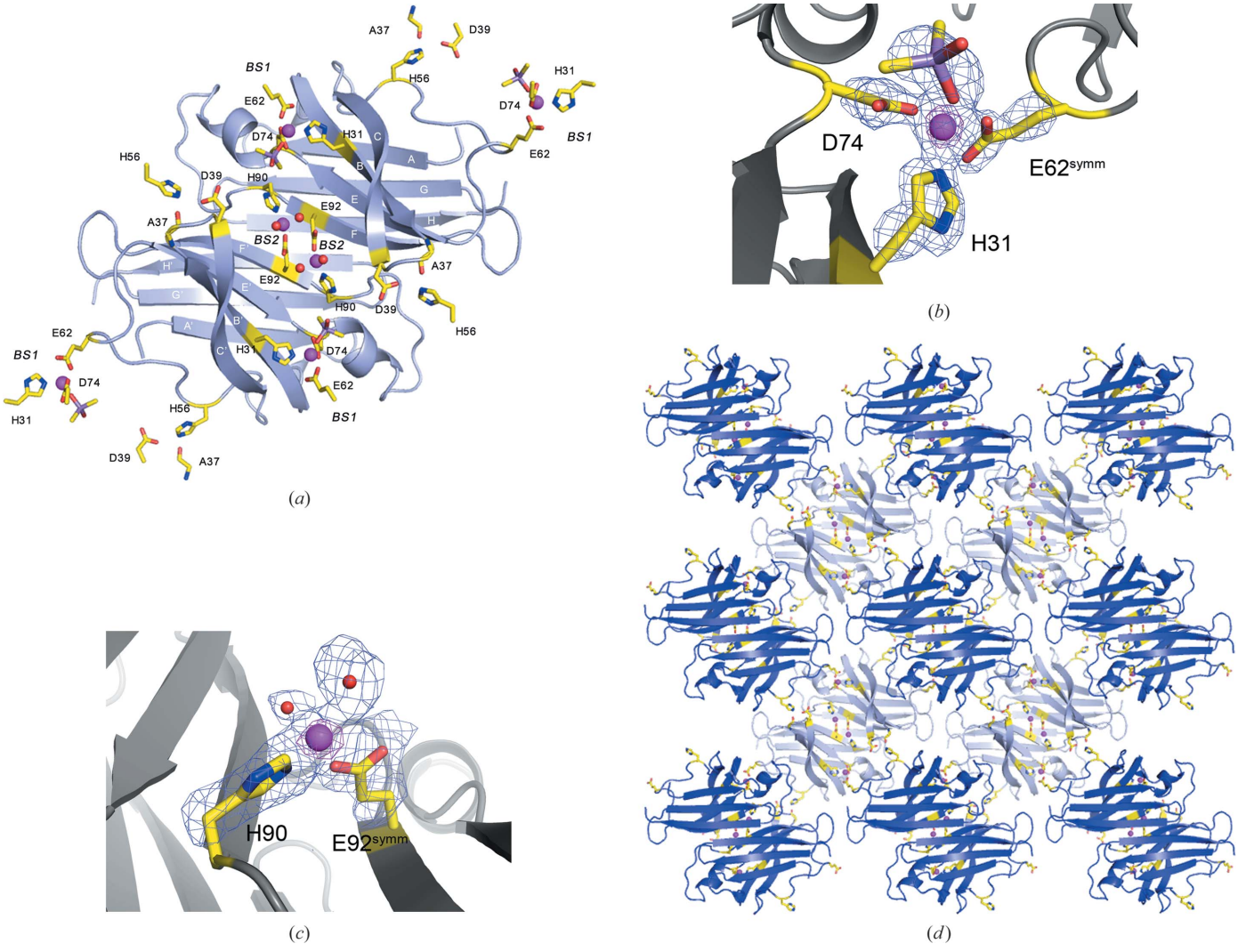

Figure 2
The Zn^{2+}-binding sites and crystal-packing interactions present in the TTR L55P–Zn^{2+} complex. The Zn^{2+} ions are shown as magenta spheres and the side chains of the Zn^{2+}-coordinating residues and also the side chains or main chain (Ala37) of the other residues involved in crystal contacts are shown as sticks. The Zn^{2+}-coordinating solvent molecules are also displayed, namely two waters shown as red spheres at each BS2 and a cacodylate molecule shown as sticks at each BS1. (*a*) The TTR L55P–Zn^{2+} dimer is represented looking through the molecular *y* axis of the tetramer. BS1 and BS2 are indicated and the TTR L55P β-strands are labelled. This figure corresponds to a close-up view of the dimers coloured identically as in Fig. 2(*d*). (*b*) BS1 Zn^{2+}-binding site. Close-up view of the tetrahedral site showing the OMIT $F_o - F_c$ electron density at 15σ (magenta) and 1σ (light blue) contour levels. (*c*) BS2 Zn^{2+}-binding site. Close-up view of the tetrahedral site showing the OMIT $F_o - F_c$ electron density at 7σ (magenta) and 1σ (light blue) contour levels. (*d*) The two-dimensional organization of Zn^{2+}-cross-linked TTR L55P dimers as observed from the crystal packing. The Zn^{2+}-binding sites are highlighted and also the other residues from crystal-contact interactions, namely His56, Ala37 and Asp39. Dimers lying in different sides of this bilayer-like assembly are coloured differently. In this arrangement, the β-strands from symmetry-related monomers have the same orientation and all the β-strands are almost perpendicular to the vertical direction in the paper plane, configuring a cross-β structure.

(BS2) is at the monomer–monomer interface of the TTR L55P dimer (Figs. 1 and 2). The inter-tetramer site, BS1, involves residues His31 and Asp74 from one monomer, Glu62^{symm} from a monomer belonging to a contiguous tetramer and a solvent-derived cacodylate molecule (Fig. 2*b*). The intra-dimer site, BS2, is formed by residues His90 from one monomer, Glu92^{symm} from the adjacent monomer and two water molecules (Fig. 2*c*). The latter Zn^{2+}-binding site is close and identical to the site formed at the adjacent monomer, and water-bridged hydrogen bonds are established between the carboxylic acid groups of Glu92 and Glu92^{symm}. The two BS2 sites are related by a crystallographic twofold-symmetry axis and favour the link between β-strands *F* and *F*′. Both sites (BS1 and BS2) show good electron-density peaks for Zn^{2+} and well defined electron density for the side chains involved in metal coordination. The cacodylate molecule is associated only with BS1 and shows relatively high atomic *B* values, reflecting instability. At BS2, water H_2O91 forms hydrogen bonds to His90, Glu92^{symm} and the other Zn^{2+}-coordinating water, H_2O86. The latter is favourably positioned for the formation of a hydrogen-bond network involving residues His90, Glu92, Glu72 and Lys70. Overall, the Zn^{2+}-coordination distances are within the values described in previously determined structures and only H_2O91 in BS2 lies beyond the established reference values (Harding, 2006). Both Zn^{2+}-binding sites are close to ideal tetrahedral geometry.

Overall, each TTR L55P–Zn^{2+} monomer is involved in the formation of four Zn^{2+}-binding sites in which Zn^{2+} is shared between two coordinating monomers. On average, there are two Zn^{2+} ions per monomer, although the Zn^{2+}-binding sites are not fully occupied in the crystal. Refinement of the occupancies indicates 0.8 occupancy for the Zn^{2+} and coupled cacodylate ion at BS1 and 0.5 occupancy for the Zn^{2+} ions at the monomer–monomer interface of the dimer (BS2).

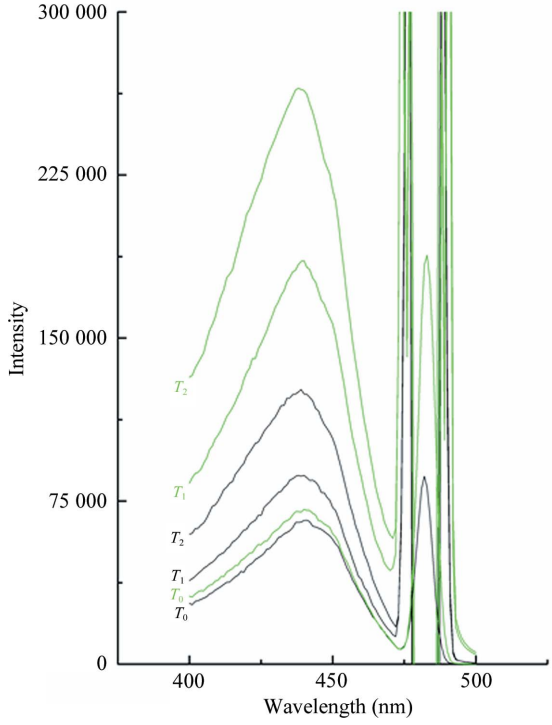

Figure 3
Effect of Zn^{2+} on TTR L55P amyloid formation as detected by fluorescence spectroscopy. ThT excitation spectra collected at different times of incubation of TTR L55P at 310 K and in the absence (black) or presence (green) of Zn^{2+}: T_0 (immediately after the incubation of the protein solution with Zn^{2+}), T_1 (after 5 d) and T_2 (after 11 d). Fluorescence intensities in each plot were corrected with the values obtained for the blank solution (in the absence of protein). Plots were generated using the *OriginPro* software (OriginLab).

3.3. Modulation of crystallization by Zn^{2+}

The Zn^{2+} ion acted as a potent additive in the crystallization of TTR L55P, inducing nucleation and fast crystal-growth kinetics. The presence of Zn^{2+} in the crystallization conditions was essential for the growth of well diffracting crystals in a narrow range of low-millimolar concentrations (3–5 m*M*) of zinc acetate. This indicated that the Zn^{2+}-coordination sites underlying crystal formation correspond to high-affinity Zn^{2+}-binding sites in the TTR L55P protein.

The effect of Zn^{2+} on the crystallization of TTR L55P can be explained by analysis of the crystallographic packing. The TTR L55P tetramers are distributed in layers and contiguous TTR L55P dimers reside on alternate sides of a bilayer-like assembly. Each TTR L55P dimer is surrounded by four dimers and the interfaces are all identical (Fig. 2*d*). This important contact region contains the BS1 Zn^{2+}-coordination sphere, namely the triad of residues His31^{symm}–Glu62–Asp74^{symm}, and hydrogen bonds established between His56 and the main chains and side chains of residues Ala37^{symm} and Asp39^{symm}, which belong to loop *BC* of a neighbouring molecule. The latter contact involves the region corresponding to β-strand *D* of the extended loop *CE*, which is characteristic of the TTR L55P variant, suggesting a TTR variant-specific packing. The bidimensional arrangement of Zn^{2+}-cross-linked TTR L55P dimers has the β-strands always with the same orientation, favouring a cross-β-like pattern, which is evident in Fig. 2(*d*). Owing to the high energy associated with metal-coordination bonds, the formation of BS1 constitutes the main force that brings together soluble TTR L55P tetramers and maintains the contacts between the dimers, while BS2 contributes to lattice integrity by stabilizing the TTR L55P dimer. This points to a direct role of Zn^{2+} in modulating both the nucleation and symmetry of the TTR L55P–Zn^{2+} crystals.

3.4. Amyloidogenic species induced by Zn^{2+}

Amyloid fibril formation resulting from the incubation of TTR L55P at 310 K in the presence or absence of Zn^{2+} was analysed using ThT and electron microscopy.

The results of the ThT-binding assay over two weeks of incubation reveal that Zn^{2+} rapidly promotes TTR L55P amyloid formation under solution conditions similar to those in which the crystals were obtained (Fig. 3). The TTR L55P solution used in the crystallization trials showed a basal level of amyloid ThT excitation signal in the absence of Zn^{2+} (at T_0), as previously reported (Sebastião *et al.*, 2000). This signal

(excitation maxima at 440 nm) increased progressively with time during incubation at 310 K, but in the presence of Zn^{2+} the ThT fluorescence showed significant further increments. These results agree with the previously reported enhancer effect of Zn^{2+} in TTR L55P amyloidogenesis (Wilkinson-White & Easterbrook-Smith, 2007).

The TEM analysis of TTR L55P under fibril-growth conditions is presented in Fig. 4. The initial samples (Fig. 4*a*) already showed the presence of oligomers/protofilaments, as expected from the ThT-binding assay results. On the third day of incubation (Fig. 4*b*) 12–13 nm wide matured fibrils were observed in the presence of Zn^{2+}, while only short oligomers/protofilaments were present in the control. Although their dimensions correspond to those of the mature fibrils, these species are still flexible and not yet structurally uniform. At a later stage of fibril growth (Fig. 4*c*; after 25 d), the fibrils obtained in the presence of Zn^{2+} are wider (14 nm) and display a more defined and rigid structure when compared with those obtained without Zn^{2+} (10 nm wide). Overall, Zn^{2+} accelerates the TTR L55P amyloidogenesis process, leading to the earlier formation of structurally defined fibrils which seem to evolve into mature fibrils with a different morphology to those obtained in the absence of Zn^{2+}.

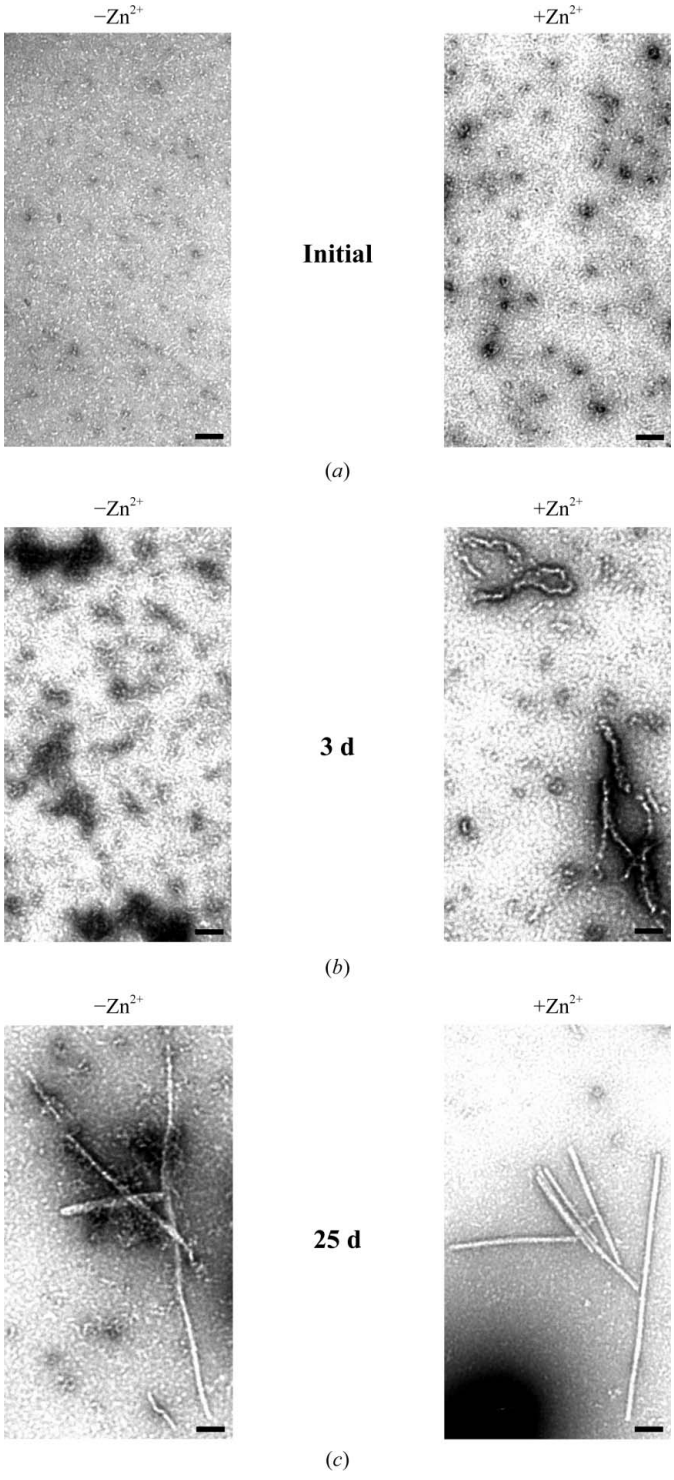

Figure 4
Effect of Zn^{2+} on TTR L55P fibril growth as visualized by TEM. Negative-stain TEM images recorded at different times of incubation of TTR L55P at 310 K in the absence or presence of Zn^{2+}. (*a*) Initial: $t = 0$. (*b*) After 3 d. (*c*) After 25 d. The scale bar in all images represents 100 nm.

4. Discussion

The Zn^{2+} concentration in human serum is approximately 15 μ*M* (Ibs & Rink, 2003; Maret, 2001) and it has been reported that it may trigger fibrillization, specifically of L55P variant TTR (Wilkinson-White & Easterbrook-Smith, 2007). Moreover, Zn^{2+} has been found in amyloid deposits extracted from the vitreous humour of FAP patients (Susuki *et al.*, 2008).

The crystal structure of the TTR L55P–Zn^{2+} complex revealed two Zn^{2+}-binding sites, BS1 and BS2, both of which bridge distinct monomers and catalyze the formation of a planar structure with all the β-strands running approximately in the same direction. Moreover, we confirmed that under conditions close to those used for crystallization, and which are near-physiological, Zn^{2+} accelerates TTR L55P fibrillization. Furthermore, the morphology of the fibrils seems to be sensitive to the presence or absence of Zn^{2+}.

While binding site BS1 provides a packing effect, BS2 plays a role in TTR L55P quaternary structure, since there are two Zn^{2+} ions that lie at the monomer–monomer interface of the dimer, strengthening the extended *CBEFF′E′B′C′* β-sheet. This effect is structurally significant since in the absence of Zn^{2+} this extended β-sheet is maintained mainly by inter-main-chain water-mediated hydrogen bonds, while the *AGH′H′G′A′* β-sheet is stabilized by direct inter-main-chain hydrogen bonds at the interface of the two *H* strands. In fact, a nuclear magnetic resonance study on TTR indicated high instability at the monomer–monomer interface of the dimer, particularly for the TTR L55P variant (Liu *et al.*, 2002). In this study we show that the effect of BS2 is reflected in the maintenance of the monomer–monomer interface, favouring the TTR L55P dimer assembly. A Zn^{2+}-binding site similar to BS2 is also found in the structure of the collagenase-3 (MMP-13) catalytic domain, providing the connection of two monomers in the crystal (Kohno *et al.*, 2006). Recently, the structure of the TTR F87M/L110M–Zn^{2+} complex has been determined (Palmieri *et al.*, 2010) and shows four Zn^{2+}-binding

sites (ZBS1–4). ZBS1, consisting of Cys10, His56 and two water molecules, is not present in our structure, probably because His56 is next to the L55P mutation, which introduces large structural modifications in this region. In contrast, His90 and Glu92 are involved in Zn^{2+} binding in both structures, although the binding sites are different. In the case of TTR F87M/L110M, the side chains of His88, His90 and Glu92 provide an intramonomer Zn^{2+}-binding site (ZBS2), while in TTR L55P–Zn^{2+} we observe an intermonomer site (BS2) provided by the side chains of His90 and Glu92 and two water molecules, which is located at the dimer interface. This difference is most likely to be a consequence of the altered monomer–monomer interface of the constructed variant TTR F87M/L110M dimer (Jiang *et al.*, 2001). The BS1 site, which is responsible for the packing of the TTR L55P molecules, is formed by His31, Asp74, Glu62 from a symmetry-related tetramer and one solvent molecule. This binding site also occurs in the case of the constructed variant (referred to as ZBS3′), but only in some subunits of the structures obtained at pH 7.5, 6.5 and 5.5 and in all subunits at pH 4.6, indicating that acidification renders this molecule into a structure more similar to TTR L55P in this region. Finally, the described ZBS4 binding site involves His31 and Asp74 from one molecule and Glu61 from a symmetry-related tetramer. This reveals significant differences between the two variant proteins, with Zn^{2+} not being able to influence the crystal packing as described here for TTR L55P.

As shown by TEM and ThT binding, Zn^{2+} induces a much faster process for TTR L55P amyloid formation under conditions similar to those under which the TTR L55P–Zn^{2+} tetragonal crystals were obtained. Furthermore, TEM analysis of late-stage fibrils reveals fibrils that seem to have a different morphology in the presence or absence of Zn^{2+}. They achieve a more advanced maturation stage in the presence of Zn^{2+}, which is a consequence of the catalytic role of the ion. The observed bidimensional cross-β-like arrangement of TTR L55P dimers as revealed by the TTR L55P–Zn^{2+} crystal packing (Fig. 2*d*) suggests that Zn^{2+} has the ability to promote an amyloid-like assembly by mediating the formation of early intermediate species, which are planar and have nearly a cross-β structure. These planar assemblies may twist upon themselves, forming hollow tubular structures resembling the fibrils shown in Fig. 4 (after 25 d). Interestingly, these fibrils seem to be similar to the TTR V30M amyloid fibrils extracted from vitreous humour (Cardoso *et al.*, 2002). The same authors also reported that the fibrils obtained from vitreous humour and those extracted from a biopsy of the peripheral nerves had different dimensions and morphology; they suggested that polymorphism of the TTR fibrillar assemblies occurs *in vivo*. Importantly, Zn^{2+} was reported to occur in amyloid deposits extracted from the vitreous humour of FAP patients, being the main metal (Susuki *et al.*, 2008). Moreover, it has been reported that Zn^{2+} can control the rate of self-assembly of the Alzheimer β-peptide (Aβ) and regulate amyloid morphology *via* distinct coordination environments (Dong *et al.*, 2006). In our assay, the TTR L55P fibrils assembled in the absence of Zn^{2+} (after 25 d), or in its presence after 3 d, resembled those produced in the absence of the ion in the previous study (Cardoso *et al.*, 2002), which were up to 8 nm wide and displayed a flexible structure. These fibrils (TTR L55P without Zn^{2+} after 25 d) are more closely related in morphology to those extracted from peripheral nerves.

Checking all the different crystal packings of human TTR structures deposited in the PDB confirmed that the arrangement that we observed is only present in the TTR L55P–Zn^{2+} tetragonal packing and is a consequence of the Zn^{2+}-binding sites. The novel TTR L55P–Zn^{2+} structure is also unique in having just the monomer in the asymmetric unit and complements the spectrum of packing possibilities previously described for TTR (Cody & Wojtczak, 2009). Comparison of the crystallographic packing present in the available structures of the TTR L55P variant, it is clear that binding site BS1 is crucial for the molecular arrangement since it restricts crystal contact possibilities and in our case led to one single molecular interface, as shown in Fig. 2(*d*). In the orthorhombic packing (PDB entry 3djz, Cendron *et al.*, 2009; PDB entry 2b14, Morais-de-Sá *et al.*, 2006), although the residues His31^{symm}–Glu62–Asp74^{symm} which form BS1 in our structure (see Fig. 2*a*) are closely positioned, Ala37/Asp39 and His56^{symm} are exposed to the solvent and are kept apart by the interactions of the crystalline arrangement. In the monoclinic packing (PDB code 5ttr; Sebastião *et al.*, 1998) Glu62 forms a contact with His56^{symm}.

The rates of urea-mediated dissociation of the TTR tetramer in the presence and absence of Zn^{2+} at molar ratios Zn^{2+}/TTR L55P similar to those used by us for crystallization have been studied (Wilkinson-White & Easterbrook-Smith, 2007). It was reported that Zn^{2+} enhances the rate of dissociation of TTR L55P tetramers, shifting the equilibrium of species in solution away from the native tetrameric state and thereby promoting amyloid formation. Our observations suggest that upon TTR L55P tetramer dissociation Zn^{2+} mediates the formation of a new monomer interface through BS1, which is crucial for the assembly of amyloidogenic intermediates whose internal order is closer to the amyloid fibril structure. In fact, the TTR L55P monomers assemble using BS1 and BS2 as interfaces and form additional contacts that privilege an amyloid-like polymerization. This defines an alternative Zn^{2+}-dependent TTR L55P amyloidogenesis pathway that involves native-like TTR L55P dimers as modular units of the amyloidogenic intermediates. Interestingly, the two BS2 sites are very close to each other and the occupancy of Zn^{2+} is 0.5, indicating that only half of the Zn^{2+}-binding sites are occupied. Consequently, the native-like dimer is not a very rigid structure and instead has some flexibility. There is some controversy in the literature concerning the presence or not of dimers in TTR amyloid fibrils (Damas & Saraiva, 2000) and this is probably related to the reported polymorphism of amyloid fibrils. It is conceivable that the type of interactions established between the two monomers in a dimer, which determine its flexibility, also determine the structure of the fibrils. Evidence from site-directed spin-labelling (SDSL) studies reveals the maintenance of the native β-strand *FF′* interface in TTR amyloid fibrils (Serag *et al.*,

2001). If this concept applies to TTR L55P–Zn^{2+} amyloid fibrils, the role of BS2 in stabilizing the TTR L55P dimer may contribute to the integrity of the amyloidogenic intermediate structural unit, the TTR L55P–Zn^{2+} dimer. In fact, it was possible to isolate an amyloidogenic dimer from the constructed variant TTR V14N/V16E (Olofsson *et al.*, 2001). Nonetheless, different engineered disulfide-bonded wt TTR dimers were non-amyloidogenic after low-pH incubation (Redondo *et al.*, 2000). On the whole, these results reflect variability in the amyloidogenic behaviour of different dimeric conformers. The decisive role of Zn^{2+} in promoting specific amyloidogenic contacts will be dependent on the particular TTR conformation. Rearrangements of the observed TTR L55P–Zn^{2+} association would be required to bring it in line with the recently proposed TTR fibril models derived from SDSL and NMR studies, which implicate the displacement of the edge strands *C* and *D* and the subsequent formation of a *BB*′ intermolecular interface in a continuous $(BEFF'E'B')_n$ β-sheet at the core of the fibril (Serag *et al.*, 2002) or the assembly of a continuous β-sandwich $(BEFF'E'B'/AGHH'G'A')_n$ (Gales *et al.*, 2007; Olofsson *et al.*, 2004). Nonetheless, measurements from the crystallographic packing shown in Fig. 2(*d*) revealed that two contiguous monomers along an axis perpendicular to the β-strands have a mean rise value of 27.3 Å, which is close to the 29 Å period determined for vitreous amyloid fibrils analysed by X-ray diffraction (Inouye *et al.*, 1998).

Zn^{2+} has recently been shown to induce the aggregation and enhance the rate of amyloid formation by TTR L55P but not by wt TTR upon incubation at 310 K and a non-acidic pH (Wilkinson-White & Easterbrook-Smith, 2007). The requirement for acidic conditions for amyloid fibril formation by wt TTR indicate that the Zn^{2+}-dependent amyloidogenesis mechanism proposed here for TTR L55P may not be possible for the wt TTR structure. In principle, wt TTR can also form the BS2 site. Nonetheless, the conformation of the β-strand *D* region in the wt TTR structure does not allow optimization of the molecular interface containing BS1 or the interactions between His56 and Ala37/Asp39 from different monomers (Fig. 2*d*), which may hamper its assembly into the packing described here for TTR L55P. In summary, the conformation of the region corresponding to β-strand *D* in TTR L55P may play a decisive role in facilitating the packing of TTR L55P molecules into a cross-β-like arrangement promoted by Zn^{2+} binding, which may be associated with the high amyloidogenic behaviour of this variant. In fact, it was shown in the same study that the double mutant TTR L55P/H56G impairs Zn^{2+}-induced enhancement of amyloid formation when compared with TTR L55P, even though it has similar Zn^{2+}-binding affinity and aggregation properties, arguing in favour of the importance given by us to the interaction involving His56 and Ala37/Asp39 in the packing.

Metal ions have been implicated in pathological mechanisms underlying different amyloidogenic diseases, namely by interactions with the Aβ peptide (Bush, 2003), β_2-microglobulin (β2m; Calabrese & Miranker, 2009), PrP in prion diseases (Millhauser, 2007) and α-synuclein in Parkinson's disease (Uversky *et al.*, 2001). There are reports of the formation of oligomers owing to the catalytic role of Zn^{2+} bridging different molecules, as happens for insulin hexamers (Baker *et al.*, 1988) and amyloid Aβ peptide (Tsvetkov *et al.*, 2010). The influence of Zn^{2+} on TTR L55P amyloidogenesis described here corresponds to an effect on quaternary structure owing to a packing modulation, without affecting the protein conformation, which is already in an amyloidogenic state. The reported TTR L55P–Zn^{2+} crystallographic structure reveals a possible alternative and enhanced mechanism of TTR amyloidogenesis, offering important leads for the development of novel anti-amyloid drugs by addressing new potential pathologic characteristics.

We thank Paul Moreira for excellent technical assistance in the preparation of the recombinant TTR L55P variant, Dr João Morais Cabral for help in X-ray diffraction data collection, the staff at beamline ID14-2 of the ESRF for technical assistance, Dr Frederico Silva for help with ThT fluorescence data collection and Rui Fernandes for the electron microscopy analysis. This work was supported by grants from Fundação para a Ciência e Tecnologia, Portugal (POCI/V.5/A0117/2005) and European Union project EURAMY (FP6-2006–037525).

References

Almeida, M. R. & Saraiva, M. J. (1996). *Eur. J. Endocrinol.* **135**, 226–230.
Andrade, C. (1952). *Brain*, **75**, 408–427.
Baker, E. N., Blundell, T. L., Cutfield, J. F., Cutfield, S. M., Dodson, E. J., Dodson, G. G., Hodgkin, D. M., Hubbard, R. E., Isaacs, N. W., Reynolds, C. D., Sakabe, K., Sakabe, N. & Vijayan, N. M. (1988). *Philos. Trans. R. Soc. Lond. B Biol. Sci.* **319**, 369–456.
Blake, C. C., Geisow, M. J., Oatley, S. J., Rérat, B. & Rérat, C. (1978). *J. Mol. Biol.* **121**, 339–356.
Blake, C. & Serpell, L. (1996). *Structure*, **4**, 989–998.
Brunger, A. T. (2007). *Nature Protoc.* **2**, 2728–2733.
Bush, A. I. (2003). *Trends Neurosci.* **26**, 207–214.
Calabrese, M. F. & Miranker, A. D. (2009). *Prion*, **3**, 1–4.
Cardoso, I., Goldsbury, C. S., Müller, S. A., Olivieri, V., Wirtz, S., Damas, A. M., Aebi, U. & Saraiva, M. J. (2002). *J. Mol. Biol.* **317**, 683–695.
Cendron, L., Trovato, A., Seno, F., Folli, C., Alfieri, B., Zanotti, G. & Berni, R. (2009). *J. Biol. Chem.* **284**, 25832–25841.
Cody, V. & Wojtczak, A. (2009). *Recent Advances in Transthyretin Evolution, Structure and Biological Functions*, edited by S. D. Richardson & V. Cody, pp. 1–21. New York: Springer-Verlag.
Damas, A. M. & Saraiva, M. J. (2000). *J. Struct. Biol.* **130**, 290–299.
Dong, J., Shokes, J. E., Scott, R. A. & Lynn, D. G. (2006). *J. Am. Chem. Soc.* **128**, 3540–3542.
Eanes, E. D. & Glenner, G. G. (1968). *J. Histochem. Cytochem.* **16**, 673–677.
Emsley, P. & Cowtan, K. (2004). *Acta Cryst.* D**60**, 2126–2132.
Furuya, H., Saraiva, M. J., Gawinowicz, M. A., Alves, I. L., Costa, P. P., Sasaki, H., Goto, I. & Sakaki, Y. (1991). *Biochemistry*, **30**, 2415–2421.
Gales, L., Cardoso, I., Fayard, B., Quintanilha, A., Saraiva, M. J. & Damas, A. M. (2003). *J. Biol. Chem.* **278**, 11654–11660.
Gales, L., Saraiva, M. J. & Damas, A. M. (2007). *Biochim. Biophys. Acta*, **1774**, 59–64.
Ghayour-Mobarhan, M., Taylor, A., New, S. A., Lamb, D. J. & Ferns, G. A. (2005). *Ann. Clin. Biochem.* **42**, 364–375.

Goldsteins, G., Andersson, K., Olofsson, A., Dacklin, I., Edvinsson, A., Baranov, V., Sandgren, O., Thylén, C., Hammarstrom, S. & Lundgren, E. (1997). *Biochemistry*, **36**, 5346–5352.
Harding, M. M. (2006). *Acta Cryst.* D**62**, 678–682.
Ibs, K.-H. & Rink, L. (2003). *J. Nutr.* **133**, 1452S–1456S.
Inouye, H., Domingues, F. S., Damas, A. M., Saraiva, M. J., Lundgren, E., Sandgren, O. & Kirschner, D. A. (1998). *Amyloid*, **5**, 163–174.
Jacobson, D. R., McFarlin, D. E., Kane, I. & Buxbaum, J. N. (1992). *Hum. Genet.* **89**, 353–356.
Jiang, X., Smith, C. S., Petrassi, H. M., Hammarström, P., White, J. T., Sacchettini, J. C. & Kelly, J. W. (2001). *Biochemistry*, **40**, 11442–11452.
Kohno, T., Hochigai, H., Yamashita, E., Tsukihara, T. & Kanaoka, M. (2006). *Biochem. Biophys. Res. Commun.* **344**, 315–322.
Lashuel, H. A., Wurth, C., Woo, L. & Kelly, J. W. (1999). *Biochemistry*, **38**, 13560–13573.
Leslie, A. G. W. (1992). *Jnt CCP4/ESF–EACBM Newsl. Protein Crystallogr.* **26**.
Liu, K., Kelly, J. W. & Wemmer, D. E. (2002). *J. Mol. Biol.* **320**, 821–832.
Maret, W. (2001). *Proc. Natl Acad. Sci. USA*, **98**, 12325–12327.
McCoy, A. J., Grosse-Kunstleve, R. W., Adams, P. D., Winn, M. D., Storoni, L. C. & Read, R. J. (2007). *J. Appl. Cryst.* **40**, 658–674.
McCutchen, S. L., Colon, W. & Kelly, J. W. (1993). *Biochemistry*, **32**, 12119–12127.
Millhauser, G. L. (2007). *Annu. Rev. Phys. Chem.* **58**, 299–320.
Morais-de-Sá, E., Neto-Silva, R. M., Pereira, P. J. B., Saraiva, M. J. & Damas, A. M. (2006). *Acta Cryst.* D**62**, 512–519.
Olofsson, A., Ippel, H. J., Baranov, V., Hörstedt, P., Wijmenga, S. & Lundgren, E. (2001). *J. Biol. Chem.* **276**, 39592–39599.
Olofsson, A., Ippel, J. H., Wijmenga, S. S., Lundgren, E. & Ohman, A. (2004). *J. Biol. Chem.* **279**, 5699–5707.
Palaninathan, S. K., Mohamedmohaideen, N. N., Snee, W. C., Kelly, J. W. & Sacchettini, J. C. (2008). *J. Mol. Biol.* **382**, 1157–1167.
Palmieri, L. de C., Lima, L. M. T. R., Freire, J. B. B., Bleicher, L., Polikarpov, I., Almeida, F. C. L. & Foguel, D. (2010). *J. Biol. Chem.* **285**, 31731–31741.
Quintas, A., Vaz, D. C., Cardoso, I., Saraiva, M. J. & Brito, R. M. (2001). *J. Biol. Chem.* **276**, 27207–27213.
Raz, A. & Goodman, D. S. (1969). *J. Biol. Chem.* **244**, 3230–3237.
Redondo, C., Damas, A. M. & Saraiva, M. J. (2000). *Biochem. J.* **348**, 167–172.
Saraiva, M. J. (2001). *Data Base on Transthyretin Mutations.* http://www.ibmc.up.pt/mjsaraiva/ttrmut.html.
Scott, B. J. & Bradwell, A. R. (1983). *Clin. Chem.* **29**, 629–633.
Sebastião, M. P., Merlini, G., Saraiva, M. J. & Damas, A. M. (2000). *Biochem. J.* **351**, 273–279.
Sebastião, M. P., Saraiva, M. J. & Damas, A. M. (1998). *J. Biol. Chem.* **273**, 24715–24722.
Serag, A. A., Altenbach, C., Gingery, M., Hubbell, W. L. & Yeates, T. O. (2001). *Biochemistry*, **40**, 9089–9096.
Serag, A. A., Altenbach, C., Gingery, M., Hubbell, W. L. & Yeates, T. O. (2002). *Nature Struct. Biol.* **9**, 734–739.
Sunde, M., Serpell, L. C., Bartlam, M., Fraser, P. E., Pepys, M. B. & Blake, C. C. (1997). *J. Mol. Biol.* **273**, 729–739.
Susuki, S., Ando, Y., Sato, T., Nishiyama, M., Miyata, M., Suico, M. A., Shuto, T. & Kai, H. (2008). *Amyloid*, **15**, 108–116.
Tsvetkov, P. O., Kulikova, A. A., Golovin, A. V., Tkachev, Y. V., Archakov, A. I., Kozin, S. A. & Makarov, A. A. (2010). *Biophys. J.* **99**, L84–L86.
Uversky, V. N., Li, J. & Fink, A. L. (2001). *J. Biol. Chem.* **276**, 44284–44296.
Westermark, P., Sletten, K., Johansson, B. & Cornwell, G. G. III (1990). *Proc. Natl Acad. Sci. USA*, **87**, 2843–2845.
Wilkinson-White, L. E. & Easterbrook-Smith, S. B. (2007). *Biochemistry*, **46**, 9123–9132.
Winn, M. D. *et al.* (2011). *Acta Cryst.* D**67**, 235–242.
Wojtczak, A., Cody, V., Luft, J. R. & Pangborn, W. (1996). *Acta Cryst.* D**52**, 758–765.